SCIENTIFIC REPORTS

OPEN

SUBJECT AREAS:
ELECTRONIC DEVICES
SOLAR CELLS

Received
25 September 2014

Accepted
25 February 2015

Published
24 March 2015

Correspondence and requests for materials should be addressed to J.-M.T. (jting@mail.ncku.edu.tw)

Cu_2ZnSnS_4 absorption layers with controlled phase purity

Chia-Ying Su[1], Chiu -Yen Chiu[2] & Jyh-Ming Ting[1,3]

[1]Department of Materials Science and Engineering, National Cheng Kung University, Tainan, Taiwan, [2]Material and Chemical Research, Industrial Technology Research Institute, Hsinchu, Taiwan, [3]Research Center for Energy Technology and Strategy, National Cheng Kung University.

We report the synthesis and characterization of Cu_2ZnSnS_4 (CZTS) with controlled phase purity. The precursor was first prepared using sequential electrodeposition of Cu, Zn, and Sn in different orders. The Cu/(Sn+Zn) ratio in each stacking order was also varied. The precursor was subjected to annealing at 200°C and sulfurization at 500°C in a 5%-H_2S/Ar atmosphere for the formation of CZTS. The phase evolutions during the electrodeposition and annealing stages, and the final phase formation at the sulfurization stage were examined using both x-ray diffractometry and Raman spectroscopy, both of which are shown to be complimentary tools for phase identification. Detailed growth path is therefore reported. We also demonstrate by controlling the stacking order and the Cu/(Sn+Zn) ratio, CZTS with a phase purity as high as 93% is obtained.

Electrical energy generated from various thin film solar cells are of great importance due to the depleting natural resources in the earth. Among these thin film solar cells, amorphous silicon (α-Si), cadmium telluride (CdTe), and copper indium gallium selenium (CIGS) are the major non-organic solar cells[1]. CIGS thin film solar cell is attractive due to the fabrication cost and conversion efficiency (~20%)[2,3]. However, a potential drawback of CIGS thin film solar cell is that the absorber layer contains rare earth elements of In and Ga, both of which are likely to be in shortage in the future. Therefore, alternatives are being intensively sought. As a result, semiconductor materials, quaternary Cu_2ZnSnS_4 (CZTS) and $Cu_2ZnSnSe_4$ (CZTSe) compounds are receiving increasing attentions[4]. The Zn and Sn replace the In to form a chalcopyrite-like structure[5]. CZTS exhibits a high absorption coefficient ($>10^4$ cm^{-1}) and an energy gap (~1.5 eV) matching the visible light spectrum[6]. The energy band gap can also be modified through varying the phase purity and composition[7,8]. The vacuum processes used for the fabrication of CZTS absorber layers are similar to that of the CIGS and include sputter and evaporative deposition techniques. In one type of the evaporative processes, elemental Cu, Sn, and S, and binary ZnS sources are co-evaporated onto the substrates[4]. In another type, various elements (Cu, Sn, and Zn) and compounds (ZnS and SnS_2) are evaporated in sequences[9–11]. In sputter deposition techniques, both co-sputter and sequential sputter deposition have been used. There are also several non-vacuum processes reported. The first report on CZTS thin film solar cell fabricated under non- vacuum condition is a sol-gel process[12]. The obtained cell has a conversion efficiency of 1.01%. CZTS thin films were also deposited using spray pyrolysis of an aqueous solution containing cupric chloride, zinc acetate, stannic chloride, and thiourea onto substrates heated to a temperature between 643–683 K[5]. However, an amorphous ZnS layer was observed on the surface of the CZTS film and led to increased electrical resistance. ZnS as well as was found at the interface between CZTS and Mo substrate which contributes to the high short-circuit current density, high series resistance found in the resulting cells[13]. CZTS/CZTSe thin films can also be prepared from the sintering of nanoparticles, which can be made, for example, using high-temperature arrested precipitation at 280°C[14] and hot injection[15].

Another non-vacuum alternative is electroplating, which is a scalable process. Electroplating is a room-temperature process. Also, this technique eliminates the problem of residual carbon that is often arisen in other non-vacuum processes[16–18]. CZTS thin films can be obtained using co-plating or sequential plating of the constituent elements with[19,20] or without S[21–24]. Post-plating sulfurization is required for electroplated film with no sulfur. Compared to the sequential plating technique, the co-plating technique requires a longer deposition time[19,22] and more organic additives[22,25], and is difficult in maintaining the desired characteristics of the electrolyte[19]. In sequential electroplating, almost all of the CZTS absorber layers were electroplated on Mo-coated substrates with a stacking order of Cu/Sn/Zn without Ref. 25 or with Ref. 26 a Pd layer on the Mo surfaces. Recently, Cu/Zn/Sn precursor layer was prepared using a sequential plating technique[27]. The resulting CZTS cell is exhibiting the highest conversion efficiency (7.3%) among all the CZTS cells whose absorber layers are prepared

using electroplating techniques[28]. This indicates that the stacking order play an important role in the performance of the cell. However, only very limited studies, in which vacuum processes were used, have shown that the stacking order affects the morphology, composition, and phase of the resulting CZTS layer and therefore the cell performance. For example, six different stacking orders of Cu, Sn, and Zn were electron-beam evaporated onto Mo/glass substrates to create 3-layered films[29]. It was found that the resulting morphologies and compositions were different in different stacking orders, and a higher conversion efficiency can be obtained by having Cu and Sn adjacent to each other. Different stacking orders of Cu, Zn and Sn were sputter deposited to create multi-layered films[30]. It was found that some of the multi-layered films did not transform into "good quality CZTS films" after the sulfurization. Voids were observed in some of the all samples.

Regardless of the process methods, an important issue of concern is the phase purity. It is known that impurity phases lead to high series resistance and hence limit the conversion efficiency[21,51,52,57]. Surface impurity Cu_XS can be removed by KCN solution. However, the bulk impurity such as Cu_2SnS_3 ZnS, and Sn_xS_y co-exist with the Cu_2ZnSnS_4 phase[21,25,52–54] and cannot be removed by post-synthesis treatment. Despite of the recognition of the disadvantages of impurity phases, there is no report showing quantitative data[55,56,58,59]. In this study, we have prepared multi-layered precursor films having different stacking orders of Cu, Zn, and Sn. Also, in each stacking order, three different Cu/(Sn+Zn) ratios were studied. Each layer was electroplated sequentially. The obtained precursor films were then annealed and sulfurized in a closed quartz tube at elevated temperatures. Effects of the stacking order and the Cu/(Sn+Zn) ratio on the characteristics of the resulting CZTS are presented and discussed.

Results

XRD analysis (Fig. 1) shows that the as-plated CZT sample consists of Cu_6Sn_5, Cu, and Sn phases, as-plated CTZ sample consists of Cu_5Zn_8, Cu_3Sn, Cu, and Sn phases, as-plated CTZC sample consists of Cu_5Zn_8, Cu, and Sn phases, and as-plated CZCT sample films consists of Cu_5Zn_8, Cu_6Sn_5, Cu, and Sn phases. These phases are either two-element compounds or pure elements. For clarity, Table 1 summarizes the phases that were observed in different cases. As shown in the table, only Cu-Sn and/or Cu-Zn compounds were found. Also, Cu_5Zn_8 exists in all the as-plated samples, except the as-plated CZT as shown in Table 1. Furthermore, there is no elemental Zn in the as-plated CZT. The as-plated samples were then subjected to annealing at 200°C for 30 min in H_2S. Figs. 2A to 2C show the XRD patterns of the annealed samples. After the annealing, the

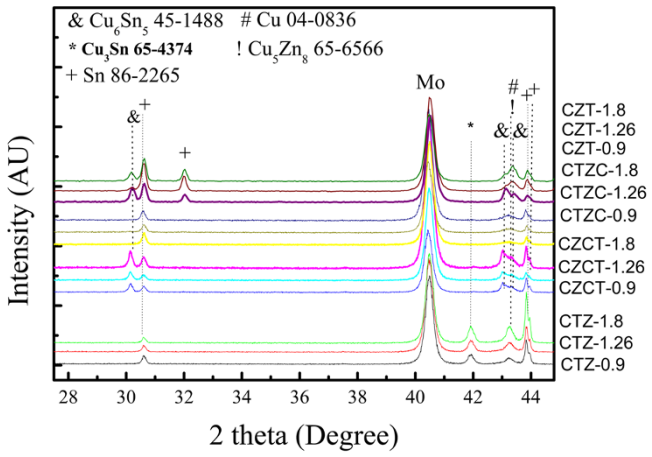

Figure 1 | XRD patterns of as-plated films. The numbers follows the sample IDs represent the Cu/(Sn+Zn) ratios.

Table 1 | XRD results of as-plated and annealing samples

	Cu_5Zn_8	Cu_6Sn_5	Cu_3Sn	Cu	Zn	Sn	Cu_2S	Sn_2S_3
As-plated CZT		X		X		X		
Annealed CZT			X	X		X		
As-plated CTZ	X		X	X		X		
Annealed CTZ	X	X	X	X				
As-plated CTZC	X			X		X		
Annealed CTCZ	X	X		X		X	X	
As-plated CZCT	X	X		X		X		
Annealed CZCT	X		X	X				X

obtained phases include Cu_5Zn_8, Cu_6Sn_5, Cu_3Sn, Cu, Sn, Cu_2S and Sn_2S_3. The results are also summarized in Table 1. In the annealed CZT, the Cu_6Sn_5 phase in the as-plated state disappears and Cu_3Sn forms after the annealing. After annealing, a new phase, i.e., Cu_6Sn_5,

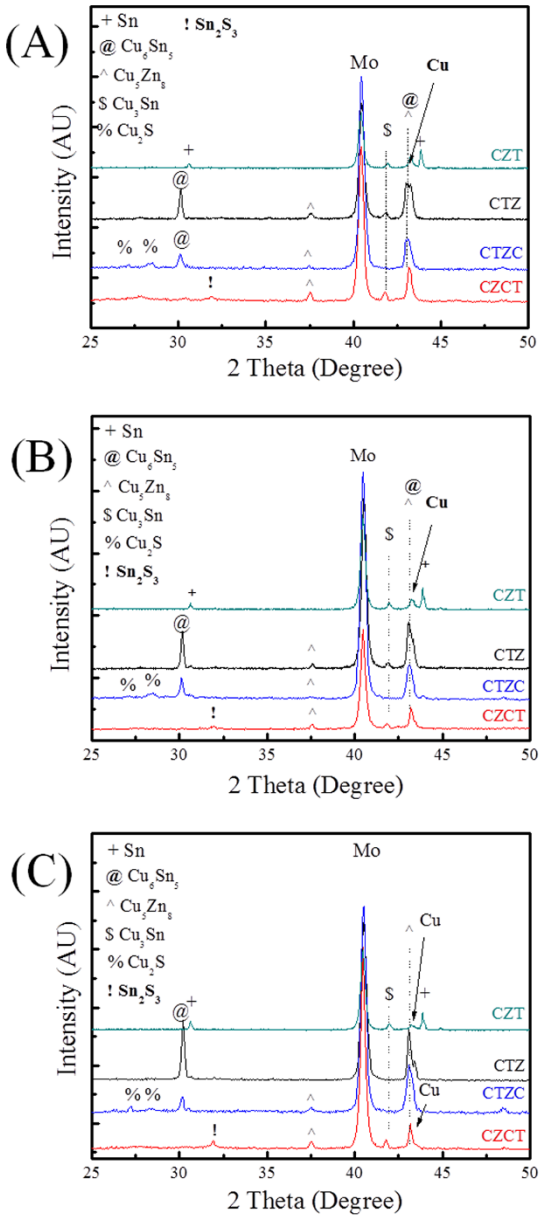

Figure 2 | XRD patterns for heat treated samples. (A) Cu/(Sn+Zn) = 1.8, (B) Cu/(Sn+Zn) = 1.26, and (C) Cu/(Sn+Zn) = 0.9. The heat treatment was performed at 200°C for 30 min in H_2S.

forms and Sn disappears in the CTZ sample. For CTZC, the annealing leads to the formation of additional phases of Cu_6Sn_5 and Cu_2S. For Sample CZCT, Cu_6Sn_5 disappears while two additional phases of Cu_3Sn and Sn_2S_3 form after the annealing. To obtain CZTS, the annealed samples were then sulfurized. After being subjected to KCN solution treatment, the sulfurized samples were analyzed. There is no obvious relation between the densification and the stacking order after the sulfurization. However, it was found that the higher the Cu/(Sn+Zn) ratio the more porous the sulfurized film as shown in Fig. 3 for selected sulfurized CTZ samples. While the phase composition of the annealed sample depends only on the stacking order but not the Cu/(Sn+Zn) ratio, the phase composition of the sulfurized sample varies with not only the stacking order but also the Cu/(Sn+Zn) ratio. Fig. 4 shows the XRD patterns of sulfurized samples. All the samples have the commonly observed surface Cu_2S[21,31], which can be removed after the KCN treatment. In the sulfurized CZT, the XRD patterns show that only CZT-0.9 and -1.26 but not CZT-1.8 have Cu_3SnS_4, SnS, and SnS_2. On the other hand, all three samples show diffractions peaks that belong to Cu_2ZnSnS_4, ZnS, and/or Cu_2SnS_3. These three phases have nearly overlapping diffraction peaks that cannot be easily indentified. However, these peaks surely belong to the kesterite structure of CZTS[32]. Although XRD is a common tool for the determination of crystalline phase, there are situations that the diffraction peaks of different phases nearly overlap, as mentioned above. Furthermore, some minor phases often cannot be detected by XRD. Therefore Raman analysis is used as a supplementary tool as reported earlier[31,33,34]. Fig. 5 gives the Raman spectra of the sulfurized samples. As mentioned above, the XRD patterns show that CZT-1.8 does not contain Cu_3SnS_4. However, a minor amount of Cu_3SnS_4 was detected by the Raman analysis. Also, Cu_4SnS_4 was not detected by the XRD but found during the Raman analysis for Samples CZT-0.9 and -1.26.

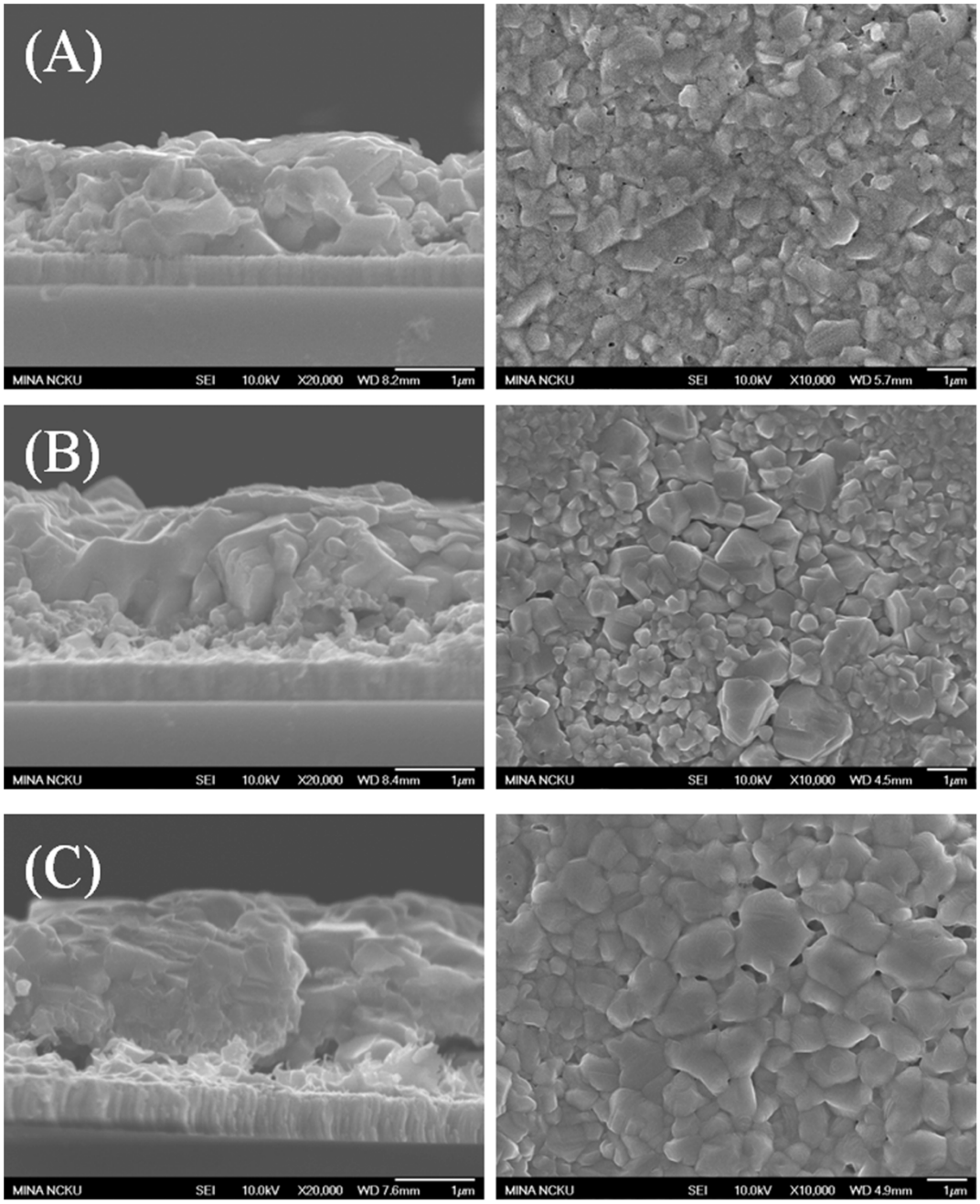

Figure 3 | **SEM cross-sectional and top view of sulfuirzed CZTS samples: (A) CTZ-0.9, (B) CTZ-1.26, and (C) CTZ-1.8.**

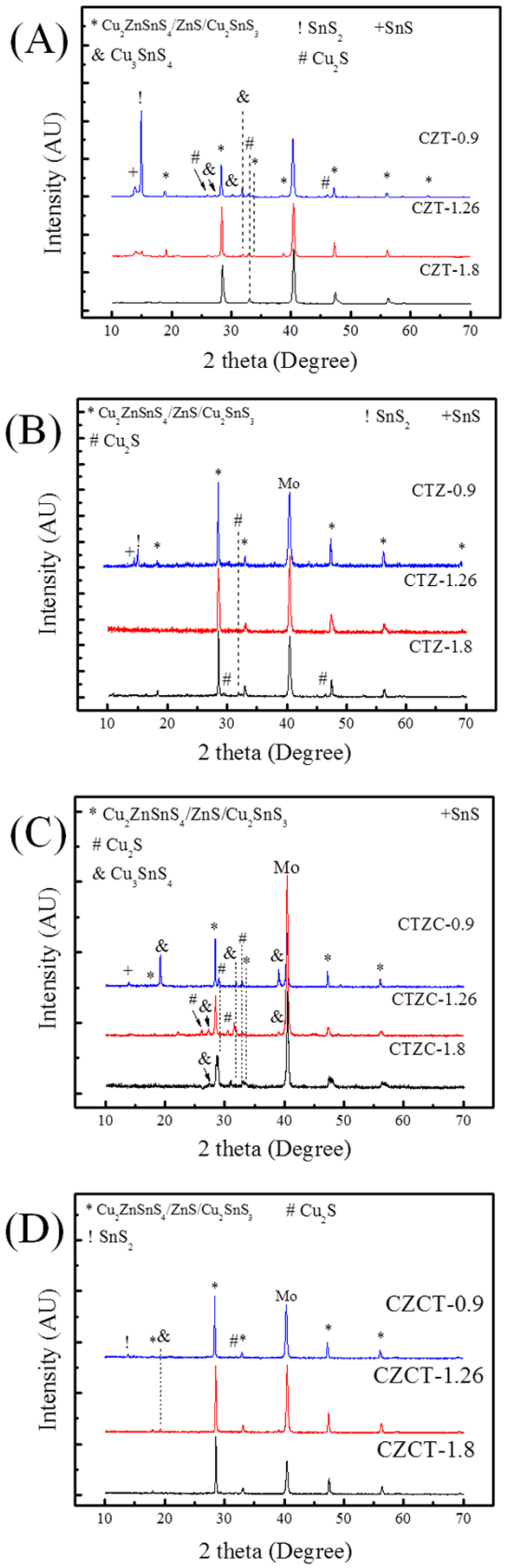

Figure 4 | XRD patterns of CZTS films. (A) CZT, (B) CTZ, (C) CTZC, and (D) CZCT.

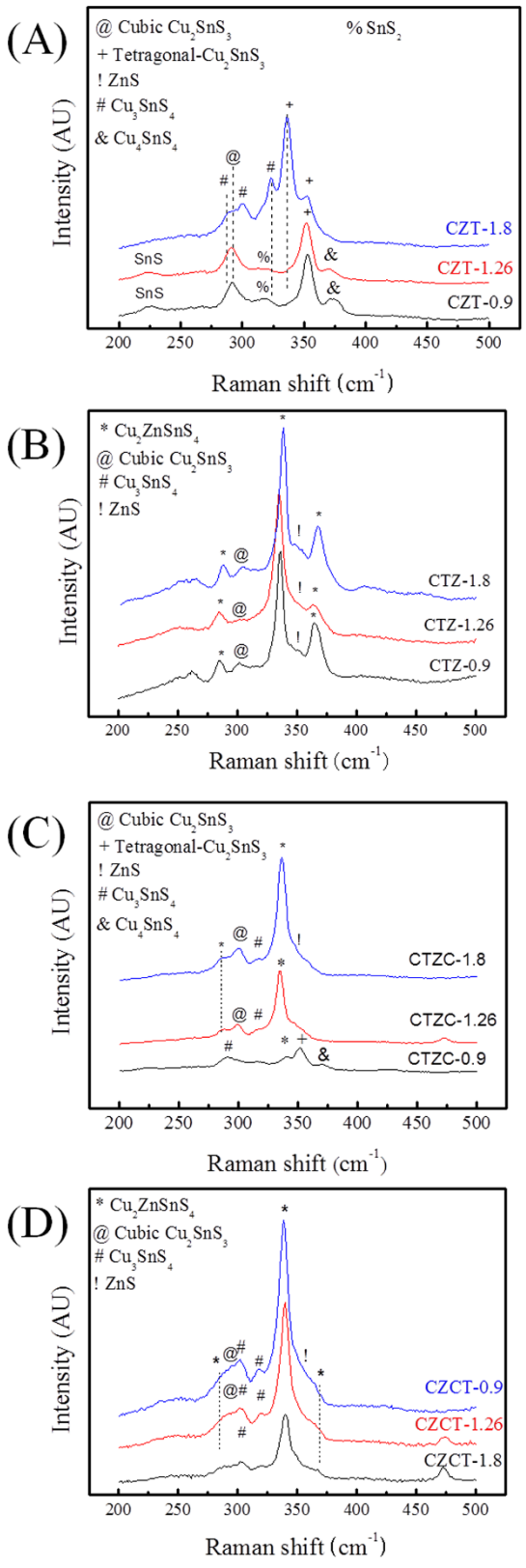

Figure 5 | Raman spectra of CZTS films. (A) CZT, (B) CTZ, (C) CTZC, and (D) CZCT.

Furthermore, although XRD cannot clearly reveal the true phase(s) of the aforementioned overlapping peaks, the Raman analysis indicates that CZT-0.9 contains only tetragonal Cu_2SnS_3 and CZT-1.26 and -1.8 contain both cubic and tetragonal Cu_2SnS_3. By the same approach, i.e., using both XRD and Raman for the phase analysis, Table 2 summarizes all the phases detected by XRD and Raman. It is apparent that some of the phases that cannot be found or identified

Table 2 | Phases identified using XRD and Raman analyses.

	Cu_2ZnSnS_4	ZnS	Cubic- Cu_2SnS_3	Tetragonal -Cu_2SnS_3	Cu_3SnS_4	Cu_4SnS_4	SnS_2	SnS
CZT-0.9				45.76%	32.58%	8.64%	8.41%	4.61%
XRD	Overlapping. Determined by Raman				Y	N	Y	Y
CZT-1.26			**6.60%**	**48.20%**	**30.30%**	**4.20%**	2.20%	8.50%
XRD	Overlapping. Determined by Raman				Y	N	Y	Y
CZT-1.8			**30.00%**	**66.20%**	**3.80%**	**0.00%**	0.00%	0.00%
XRD	Overlapping. Determined by Raman				N	N	N	N
CTZ-0.9	**78.64%**	**15.35%**	**2.69%**	**0.00%**	**0.00%**	**0.00%**	1.55%	1.78%
XRD	Overlapping. Determined by Raman				N	N	Y	Y
CTZ-1.26	**89.46%**	**9.90%**	**0.64%**	**0.00%**	**0.00%**	**0.00%**	0.00%	0.00%
XRD	Overlapping. Determined by Raman				N	N	N	N
CTZ-1.8	**93.52%**	**6.13%**	**0.36%**	**0.00%**	**0.00%**	**0.00%**	**0.00%**	**0.00%**
XRD	Overlapping. Determined by Raman				N	N	N	N
CTZC-0.9	**41.80%**	**16.30%**	**4.40%**	**0.00%**	**36.80%**	**0.00%**	0.00%	0.70%
XRD	Overlapping. Determined by Raman				Y	N	N	Y
CTZC-1.26	**46.60%**	**11.50%**	**14.40%**	**0.00%**	**27.30%**	**0.00%**	0.00%	0.20%
XRD	Overlapping. Determined by Raman				Y	N	N	Y
CTZC-1.8	**70.30%**	**3.20%**	**19.50%**	**0.00%**	**7.00%**	0.00%	0.00%	0.00%
XRD	Overlapping. Determined by Raman				Y	N	N	N
CZCT-0.9	**78.70%**	**4.30%**	**6.60%**	**0.00%**	**8.80%**	**0.00%**	1.60%	0.00%
XRD	Overlapping. Determined by Raman				N	N	Y	N
CZCT-1.26	**87.00%**	**6.50%**	**3.40%**	**0.00%**	**3.10%**	**0.00%**	0.00%	0.00%
XRD	Overlapping. Determined by Raman				N	Y	N	N
CZCT-1.8	88.10%	5.90%	3.70%	**0.00%**	2.40%	0.00%	0.00%	0.00%
XRD	Overlapping. Determined by Raman				N	N	N	N

by the XRD analysis can be realized using the Raman analysis. The phase percentage of CZTS given in Table 2 was determined from the peak area in the Raman spectra. There is no CZTS phase in sulfurized CZT. The amount of CZTS in other samples varies. It is seen that a higher Cu/(Sn+Zn) gives a higher CZTS percentage. Considering samples having different stacking orders, the CTZ group has the highest CZTS percentages, followed by the CZCT group and then the CTZC group. Furthermore, it is seen in the sulfurized CTZ-1.8, i.e., the most complete sulfurization film, there is basically no Cu_2SnS_3 (<0.4%) and only 6.1% of ZnS. TEM analysis supports this result since only CZTS and ZnS were observed as shown in Fig. 6A. A CZTS and ZnS grains are labeled as I and II, respectively. Their pertinent diffraction patterns are shown in Figs. 6B and 6C, respectively. Area I is a Cu_2ZnSnS_4 single crystal with a zone axis of [−1 1 1]. Area II is a ZnS single crystal with a zone axis of [−1 1 −1]. No cubic-Cu_2SnS_3 phase is seen which echoes the Raman analysis.

Discussion

From the above result, phase formation during each stage is schematically presently in Fig. 7. As summarized in Table 1, there is no Zn-Sn alloy or compound but only Cu-Sn and/or Cu-Zn compounds. In room temperature electrodeposited Cu-Zn samples, phases ranging from the entire spread of the binary phase diagram, including β-CuZn, γ-Cu_5Zn_8 and ε-$CuZn_5$, have been observed[35–37]. Among them, Cu_5Zn_8 is a stable room temperature phase[38]. Therefore, Cu_5Zn_8 exists in all the as-plated samples, except the as-plated CZT, which has no element Zn either. It was found that after the deposition of Cu and Zn in sequence, only Cu_5Zn_8 film was found on top of the Cu as illustrated in Fig. 7Aa and shown in Fig. S1 in the Supporting Information, indicating all the Zn reacted with the Cu. The Cu_5Zn_8 layer, however, disappeared after the subsequent pulsed plating of Sn. This is attributed to the much higher electrical resistance of Cu_5Zn_8, as compared to Cu (2 orders of magnitude higher). The high electrical resistance would create a sudden voltage drop that cracks the brittle Cu_5Zn_8 layer. In the meantime, the plated Sn reacted with the exposed Cu to form hexagonal η-Cu_6Sn_5 phase[39], leaving Sn, Cu_6Sn_5, and Cu in the sample as shown in Fig. 7Ab and Table 1. The co-existence of elemental β-Sn (tetragonal) and Cu (hexagonal), and Cu_6Sn_5 is commonly observed in electroplate Cu-Sn along with[40]. In as-plated CTZ, no Cu_6Sn_5 but Cu_3Sn, Cu_5Zn_8, Cu, and Sn were observed. Thermodynamically, Cu_6Sn_5 is more stable than Cu_3Sn[41,42]. In CTZ, after Cu and Sn were first deposited in sequence (Fig. 2Bb), the stable Cu_6Sn_5 phase was indeed identified by XRD analysis, as shown in Fig. S2 in the Supporting Information. This is also illustrated in Fig. 7Ba. Subsequent deposition of Zn then leads to not only the formation of the stable Cu_5Zn_8 phase but also the transformation of Cu_6Sn_5 to Cu_3Sn. A possible mechanism is given below and also shown schematically in Fig. 7Bb and Bc. First of all, we believe that the diffusion of Cu toward to the surface occurs during the Zn plating (Fig. 7Bb). Although such diffusion is normally induced by thermal energy[43], the pulsed power during the Zn plating could provide a driving force for the Cu diffusion. Also, the strong affinity between Cu and Zn can contribute to the diffusion. The Cu atoms that diffuse into the Cu_6Sn_5 result in excess Cu in the phase. As a result, the Cu_6Sn_5 is transformed into Cu_3Sn, as shown in Fig. 7Bc. The Cu atoms that diffuse through the Sn react with the depositing Zn to form Cu_5Zn_8, as shown in Fig. 7Bd. It is noted that the reaction between Cu and Zn is much favorable thermodynamically than that between Cu and Sn[42,44]. This is also analogous to the case of soldering, which reports that during the soldering of Sn-Zn-Ag, Sn-Zn-Ag-Al-Ga, or Sn-Bi-In-Zn onto Cu substrate, Cu diffuses into the solder and preferentially reacts with Zn to form Cu_5Zn_8[45,46]. As-plated CTZ therefore consists of Cu, Sn, Cu_5Zn_8, and Cu_3Sn (Table 1 and Fig. 7Be). In as-plated CTZ, a less stable Cu-Sn phase, i.e., Cu_3Sn, was found as mentioned above. This structure is the same as that of the as-plated CTZC before the top layer Cu plating as shown in Fig. 7Ca. After the top Cu layer plating the Cu_3Sn disappears also without the formation of any other Cu-Sn phase, as shown in Fig. 7Cb. For the as-plated CZCT, the initial plating of Cu and Zn in sequence leads to the formation of stable Cu_5Zn_8 on the remaining Cu (Fig. 7Da). Subsequent plating of additional Cu does not change the phases as shown in Fig. 7Db. Final plating of Sn then allows the reaction between the Sn and the Cu to form stable Cu_6Sn_5. As a result, as-plated CZCT consists of Cu_5Zn_8, Cu_6Sn_5, Cu, and Sn, as shown in Fig. 7Dc).

Now we discuss the annealed samples in which XRD analysis shows the existence of Cu_5Zn_8, Cu_6Sn_5, Cu_3Sn, Cu, Sn, Cu_2S and Sn_2S_3 (Table 1). The annealing of CZT leads to the disappearance of

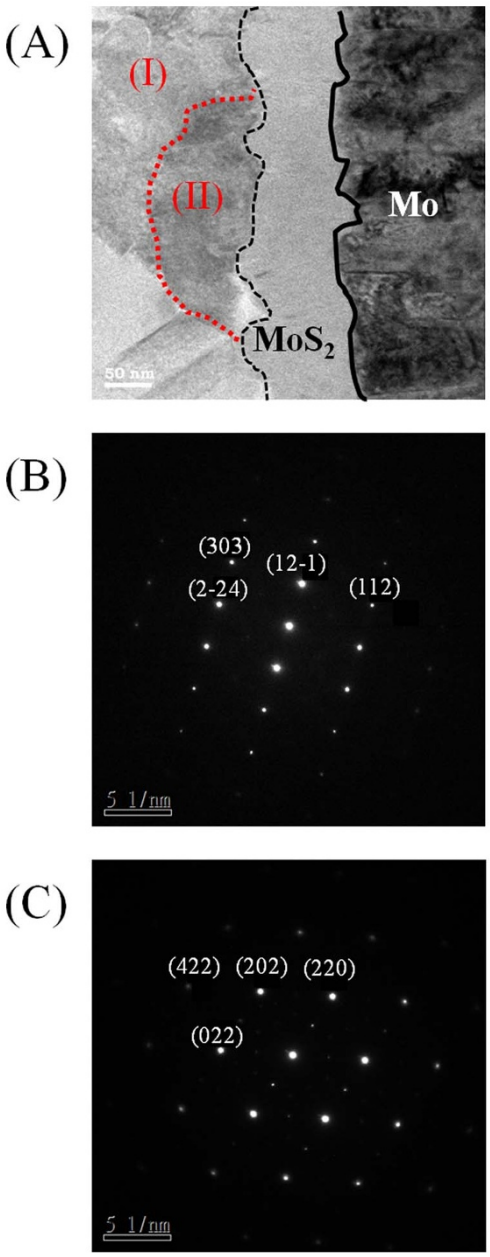

Figure 6 | TEM analysis of sulfurized CTZ-1.8sample. (A) Bright field image. (B) Diffraction patterns of areas (B) I and (C) II.

the Cu_6Sn_5. The only reason that this happened is that more Cu atoms diffuse into Cu_6Sn_5 during the annealing to form Cu_3Sn[47], as shown in Fig. 7Ac, following the mechanism that is described above during the plating. For the as-plated CTZ, Cu_6Sn_5 forms after the annealing. It is believed that Cu diffuses upwards to react with Sn to form Cu_6Sn_5 (Fig. 7Be) which is thermodynamically favorable[41]. The formation of Cu_6Sn_5 is also contributed by the reaction between Sn and Cu_3Sn[48,49], as also shown in Fig. 7Be. Both reactions, as shown in Fig. 7Be, result in the disappearance of Sn. For the as-plated CTZC (Fig. 7Cb), the annealing let the bottom Cu and Sn react to form Cu_6Sn_5, while the top Cu react with H_2S to form Cu_2S, as shown in Fig, 7Cc. For the as-annealed CZCT, two additional phases of Cu_3Sn and Sn_2S_3 were observed. As mentioned above, Cu_3Sn can be obtained through the diffusion of Cu into Cu_6Sn_5 during the annealing which also results in the disappearance of Cu_6Sn_5, as shown in Fig. 7Dd. Furthermore Sn reacts with H_2S to form Sn_2S_3 which also leads to the disappearance of Sn, as also shown in Fig. 7Dd.

The annealed samples were subsequently sulfurized to obtain CZTS. As mentioned above, no obvious relation between the densification and the stacking order after the sulfurization was observed and a higher Cu/(Sn+Zn) ratio gives a more porous sulfurized film. This is attributed to the fact that Cu reacts with sulfur easily[31]. A higher Cu/(Sn+Zn) ratio leads to more Cu/S reaction which involves the diffusion of Cu to the surface for the formation of Cu_xS (Cu_2S or CuS), leaving pores in the film. Also, after the surface Cu_xS is removed by KCN, the pores are formed too. As a result, the higher the Cu/(Sn+Zn) ratio the more porous the sulfurized film. On the other hand, the phase composition of the sulfurized sample varies with both the stacking order and Cu/(Sn+Zn) ratio. This is different from the annealed samples whose phase composition is independent of the Cu/(Sn+Zn) ratio. As mentioned above, the phase analysis was examined using both XRD and Raman and the results are shown in Table 2. It is understood that the formation of the phases in the sulfurized samples is due to the complicated interplays among many solid-state and solid-gas reactions. It is not the intention of this paper to discuss the detailed formation mechanism or the growth path. We will address here the appearance of CZTS in the sulfurized samples. From Table 2, it is seen that no CZTS phase in sulfurized CZT as there is no Zn in its as-annealed state (Table 1), while the amount of CZTS in other samples varies. Firstly, we consider the effect of Cu/(Sn+Zn) ratio, i.e., a higher Cu/(Sn+Zn) gives a higher CZTS percentage. Considering both Cu-rich and Cu-poor samples, the last stage to form CZTS is through $Cu_2SnS_3 + ZnS \rightarrow Cu_2ZnSnS_4$[23]. The formation of Cu_2SnS_3 involves reaction of $Cu_{2-x}S$ with SnS_2. In this study, a higher Cu/(Sn+Zn) ratio was obtained by increasing the Cu content. Therefore, a higher Cu/(Sn+Zn) ratio results in a higher percentage of Cu_2S, as shown in Fig. S3 in the Supporting Information. As a result, more Cu_2SnS_3 and hence more Cu_2ZnSnS_4 is obtained at a higher Cu/(Sn+Zn) ratio. Then we consider the effect of stacking orders. Comparing different stacking orders, the CTZ has the highest CZTS percentage, followed by the CZCT and then the CZT. This can be realized by also considering the last stage reaction to form CZTS shown above[23,50]. When there is no concurrent reduction of both cubic Cu_2SnS_3 and ZnS, the sulfurization is less complete, e.g., CZCT groups. For the CTCZ group, the increasing CZTS phase is accompanied by decreasing ZnS but increasing cubic Cu_2SnS_3. This indicates that the above reaction is hindered such that the CZTS phase is the lowest in the CTZC group. The most complete sulfurization group is the CTZ group where a higher percentage of CZTS is clearly accompanied by reduced percentages of both cubic Cu_2SnS_3 and ZnS in the sample. As a result, by varying the Cu/(Sn+Zn) ratio and the stacking order, the most completely sulfurized film, i.e, CTZ-1.8, has been obtained. This sample has basically no Cu_2SnS_3 (<0.4%) and only 6.1% of ZnS and its high phase purity has also been supported by TEM analysis.

Conclusions

In this study, we have investigated the formation of high phase purity CZTS through examining the effect of precursor characteristics on the phase evolutions. The precursor was prepared using sequential electrodeposition of individual layers of Cu, Sn, and Zn. Three different deposition orders were studied and in each stacking order, three Cu/(Sn+Zn) ratios were used. The electrodeposited precursor was then annealed and sulfurized in sequence in a 5%-H_2S/Ar atmosphere. It was found that the stacking order but not the Cu/(Sn+Zn) ratio affects the phase formation during the electrodeposition and annealing. However, both the stacking order and the Cu/(Sn+Zn) ratio affect the phase formation during the sulfurization. A higher Cu/(Sn+Zn) gives a higher CZTS percentage in the sulfurized sample. The effect of stacking order on the formation of CZTS phase is discussed by considering the reaction sequence. We show that the existence of and reaction among Cu_2S, Cu_2SnS_3, and ZnS determine the percentage of CZTS. Furthermore, the existence of and reaction among Cu_2S, Cu_2SnS_3, and ZnS depend on the stacking order.

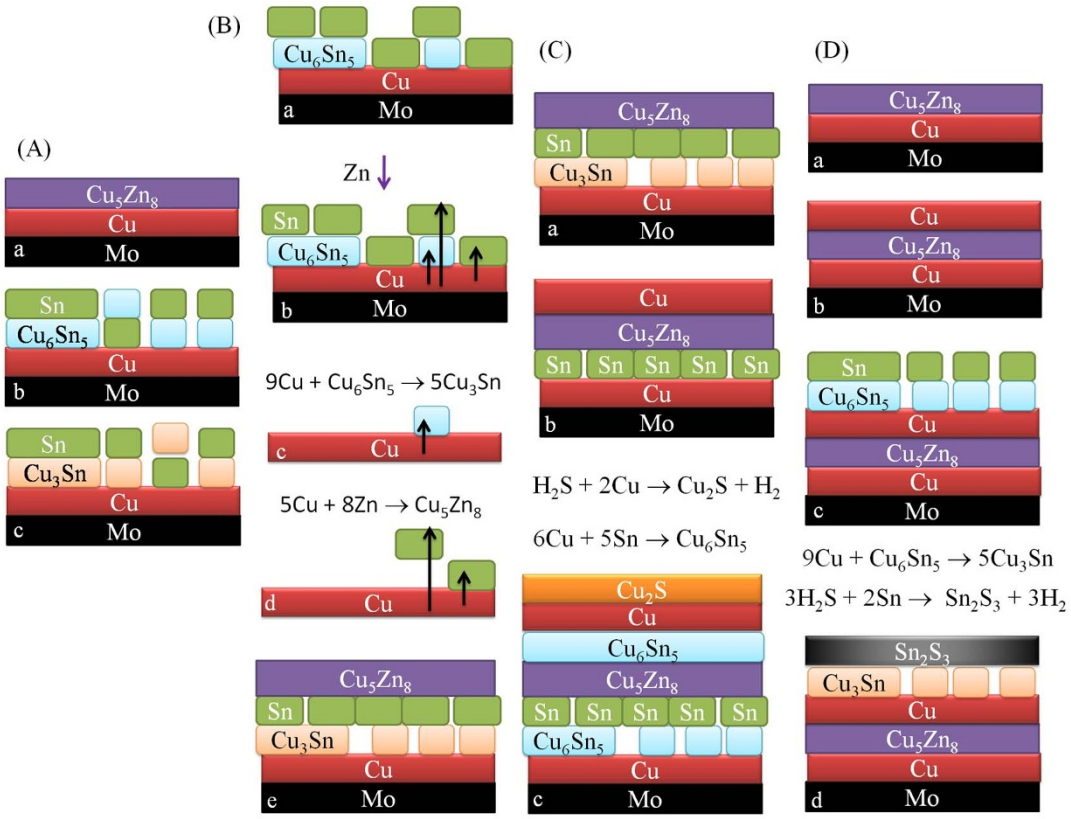

Figure 7 | Phase formation during each stage for Samples (A) CZT, (B) CTZ, (C) CTZC, and (D) CZCT.

Detailed growth path is therefore reported. We also demonstrate that by controlling the stacking order and the Cu/(Sn+Zn) ratio, CZTS with a phase purity as high as 93% can be obtained.

Methods

Copper, tin, and zinc layers were deposited on Mo-coated sodium-lime glass substrates in different sequences using an electroplating method. The electrolytes used for the plating of Cu, Zn, and Sn were 0.2 mol/L $Cu_2P_2O_7$ + 1.06 mol/L $K_4P_2O_7.H_2O$ + 9×10^{-5} mol/L SeO_2, 0.1 mol $ZnSO_4$ + 0.13 mol Na_2SO_4 + 0.06 mol H_3BO_3, and 0.1 mol $SnCl_2$ + 1.2×10^{-3} mol $CuCl_2$ + 0.16 mol $C_6H_{17}N_3O_7$, respectively. Four stacking orders were prepared for the precursors, including Cu/Zn/Sn (CZT), Cu/Sn/Zn (CTZ), Cu/Sn/Zn/Cu (CTZC), and Cu/Zn/Cu/Sn (CZCT).The total thickness of the metal precursor was 700 nm. In each type of precursor, there were three Cu/(Sn+Zn) ratios used, 0.9, 1.26, and 1.8. A high Zn/Sn atomic ratio of 1.5 was used for all the cases. A higher Zn/Sn ratio was reported to promote the formation of CZTS during sulfurization[15]. As-deposited samples are first annealed before sulfurization. Before the annealing, the quartz tube was evacuated and then back filled with 5%-H_2S/Ar until the pressure reached 400 torr. The quartz tube was then heated to 200°C for annealing. After 30-min of annealing, the heating was then continued to 500°C for sulfurization. The sulfurization time and pressure were 60 min 560 torr, respectively. The phase composition and the crystal structure of the obtained films were determined using X-ray diffraction (XRD) and Raman spectroscopy with a 100 mW He–Ne laser (wavelength 633 nm). The morphology of was examined using field emission scanning electron microscopy (FESEM). The microstructure was also examined using transmission electron microscopy (TEM).

1. Feltrin, A. & Freundlich, A. Material considerations for terawatt level deployment of photovoltaics. *Renew. energy* **3**, 180–185 (2008).
2. Repins, M. C. I. *et al.* Characterization of 19.9%-Efficient CIGS Absorbers, Paper presented at *33rd IEEE PV Specialists Conf. (PVSC): Devices and Defects*, San Diego, California. New York, USA:IEEE. (10.1109/PVSC.2008.4922628) (2008, May 11–16).
3. Repins, I. *et al.* 19·9%-efficient ZnO/CdS/CuInGaSe2 solar cell with 81·2% fill factor. *Prog. Photovolt: Res. Appl.* **16**, 235–239 (2008).
4. Katagiri, H. *et al.* Development of CZTS-based thin film solar cells. *Thin Solid Films* **517**, 2455–2460 (2009).
5. Kishore Kumar, Y. B., Suresh Babu, G., Uday Bhaskar, P. & Sundara Raja, V. Preparation and characterization of spray-deposited Cu_2ZnSnS_4 thin films. *Sol. Energy Mater. Sol. Cells* **93**, 1230–1237 (2009).
6. Yeh, M., Lee, C. & Wuu, D. Influences of synthesizing temperatures on the properties of Cu_2ZnSnS_4 prepared by sol-gel spin-coated deposition. *J. Sol-Gel Sci. Technol.* **52**, 65–68 (2009).
7. Ji, S. *et al.* A Route to Phase Controllable $Cu_2ZnSn(S_{1-x}Se_x)_4$ Nanocrystals with Tunable Energy Bands. *Sci. Rep.* **3**, 2733 (2013).
8. Fan, F. J. *et al.* Linearly arranged polytypic CZTSSe nanocrystals. *Sci. Rep.* **2**, 952 (2012).
9. Katagiri, H., Ishigaki, N., Ishida, T. & Saito, K. Characterization of Cu_2ZnSnS_4 Thin Films Prepared by Vapor Phase Sulfurization. *Jpn. J. Soc. Appl. Phys.*, **40**, 500–504 (2001).
10. Katagiri, H. Cu_2ZnSnS_4 thin film solar cells. *Thin Solid Films* **480–481**, 426–432 (2005).
11. Kobayashi, T., Tsuchid, K., Shinoda, S., Oyanagi, T. & Katagiri, H. Investigation of Cu_2ZnSnS_4-Based Thin Film Solar Cells Using Abundant Materials. *Jpn. j. appl. phys.* **44**, 783–787 (2005).
12. Tanaka, K., Oonuki, M., Moritake, N. & Uchiki, H. Thin film solar cells prepared by non-vacuum processing. *Sol. Energy Mater. Sol. Cells* **93**, 583–587 (2009).
13. Woo, K. *et al.* Band-gap-graded $Cu_2ZnSn(S_{1-x},Se_x)_4$ Solar Cells Fabricated by an Ethanol-based, Particulate Precursor Ink Route. *Sci. Rep.* **3**, 3069 (2013).
14. Steinhagen, C. *et al.* Synthesis of Cu_2ZnSnS_4 Nanocrystals for Use in Low-Cost Photovoltaics. *J. Am. Chem. Soc.* **131**, 12554–12555 (2009).
15. Guo, Q. *et al.* Fabrication of 7.2% Efficient CZTSSe Solar Cells Using CZTS Nanocrystals. *J. Am. Chem. Soc.* **132**, 17384–17386 (2010).
16. Lee, E. *et al.* Nearly carbon-free printable CIGS thin films for solar cell applications. *Sol. Energy Mater. Sol. Cells* **95**, 2928–2932 (2011).
17. Kaelin, M. *et al.* Low-cost CIGS solar cells by paste coating and selenization. *Thin Solid Films* **480–481**, 486–490 (2005).
18. Ahn, S. *et al.* $CuInSe_2$ (CIS) Thin Film Solar Cells by Direct Coating and Selenization of Solution Precursors. *J. phys. chem. C* **114**, 8108–8113 (2010).
19. Moriya, K., Tanaka, K. & Uchiki, H. Characterization of Cu_2ZnSnS_4 Thin Films Prepared by Photo-Chemical Deposition. *Jpn. j. appl. phys.* **44**, 715–717 (2005).
20. Chan, C. P., Lam, H. & Surya, C. Preparation of Cu_2ZnSnS_4 films by electrodeposition using ionic liquids. *Sol. Energy Mater. Sol. Cells* **94**, 207–211 (2010).
21. Ennaoui, A. *et al.* Cu_2ZnSnS_4 thin film solar cells from electroplated precursors: Novel low-cost perspective. *Thin Solid Films* **517**, 2511–2514 (2009).
22. Pawar, S. M. *et al.* Single step electrosynthesis of Cu_2ZnSnS_4 (CZTS) thin films for solar cell application. *Electrochim. Acta* **55**, 4057–4061 (2010).
23. Schurr, R. *et al.* The crystallisation of Cu_2ZnSnS_4 thin film solar cell absorbers from co-electroplated Cu–Zn–Sn precursors. *Thin Solid Films* **517**, 2465–2468 (2009).

24. Wang, Y. *et al.* Cu_2ZnSnS_4 films deposited by a co-electrodeposition-annealing route. *Mater. lett.* **77**, 13–16 (2012).
25. Scragg, J. J., Berg, D. M. & Dale, P. J. A 3.2% efficient Kesterite device from electrodeposited stacked elemental layers. *J. electroanal. chem.* **64**, 52–59 (2010).
26. Araki, H. *et al.* Preparation of Cu_2ZnSnS_4 thin films by sulfurizing electroplated precursors. *Sol. Energy Mater. Sol. Cells* **93**, 996–999 (2009).
27. Pourbaix, M. Atlas of Electrochemical Equilibria in Aqueous Solutions. *National Association of Corrosion Engineers (NACE), Houston, Texas, USA* (1974).
28. Ahmed, S. *et al.* A High Efficiency Electrodeposited Cu_2ZnSnS_4 Solar Cell. *Adv. Energy Mater.* **2**, 253–259 (2012).
29. Araki, H. *et al.* Preparation of Cu_2ZnSnS_4 thin films by sulfurization of stacked metallic layers. *Thin Solid Films.* **517**, 1457–1460 (2008).
30. Yoo, H. & Kim, J. Growth of Cu_2ZnSnS_4 thin films using sulfurization of stacked metallic films. *Thin Solid Films.* **518**, 6567–6572 (2010).
31. Tsai, C. H., Ting, J. M. & Wang, R. R. Microstructural analysis and phase transformation of $CuInS_2$ thin filmsduring sulfurization. *Acta Mater.* **59**, 349–354 (2011).
32. Zhang, X. *et al.* Efficient Thermolysis Route to Monodisperse Cu_2ZnSnS_4 Nanocrystalswith Controlled Shape and Structure. *Sci. Rep.* **5**, 5086 (2014).
33. Su, C. Y., Mishra, D. K., Chiu, C. Y. & Ting, J. M. Effects of Cu_2S sintering aid on the formation of $CuInS_2$ coatings from single crystal $Cu_2In_2O_5$ nanoparticles. *Surf. coat. technol.* **231**, 517–520 (2013).
34. Tsai, C. H., Mishra, D. K., Su, C. Y. & Ting, J. M. Effects of sulfurization and Cu/In ratio on the performance of the $CuInS_2$ solar cell. *Int. J. Energy Res.* **38**, 418–428 (2014).
35. Domínguez-Ríos, C. *et al.* Effect of tartrate salt concentration on the morphological characteristics and composition of Cu-Zn electroless plating on zamak 5 zinc alloy. *Surf. coat. technol.* **202**, 4848–4854 (2008).
36. Juskenas, R., Karpavičienė, V., Pakštas, V., Selskis, A. & Kapočius, V. Electrochemical and XRD studies of Cu-Zn coatings electrodeposited in solution with D-mannitol. *J. electroanal. chem.* **602**, 237–244 (2007).
37. Baker, H. [*Alloy phase Diagrams*] *ASM Handbook, Vol. 3*, [Okamoto, H.][25-383] (ASM International, Materials Park, USA, Ohio, 1992).
38. Tu, K. N. Cu/Sn interfacial reactions: Thin-film case versus bulk case. *Mater. chem. phys.* **46**, 217–223 (1996).
39. Carlos, I. A. *et al.* Study of the influence of the polyalcohol sorbitol on the electrodeposition of copper-zinc films from a non-cyanide bath. *J. appl. electrochem.* **30**, 987–994 (2000).
40. Hultgren, R., Desai, P. D., Hawkins, D. T., Gileiser, M. & Kelley, K. K. [Cu-Sn, Copper-Tin] Selected Values of the Thermodynamic Properties of Binary Alloy [Hultgren, R. R.][795–800] (American Society for Metals, Metals Park, Ohio, 1973).
41. Wang, M. C., Yu, S. P., Chang, T. C. & Hon, M. H. Formation and morphology of the intermetallic compounds formed at the 91Sn–8.55Zn–0.45Al lead-free solder alloy/Cu interface. *J. Alloys Compd.* **389**, 133–139 (2005).
42. Chou, C. Y. & Chen, S. W. *Phase equilibria of the Sn-Zn-Cu ternary system. Acta Mater.* **54**, 2393–2400 (2006).
43. Yu, S. P., Wang, M. C. & Hon, M. H. Formation of intermetallic compounds at eutectic Sn–Zn–Al solder/Cu interface. *J. Mater. Res.* **16**, 76–82 (2001).
44. Yu, D. Q. *et al.* Electromigration Study of 50 μm Pitch Micro Solder Bumps using Four-Point Kelvin Structure. Paper presented at *Electronic Components and Technology Conference,* San Diego, CA. New Jersey, United States: Institute of Electrical and Electronics Engineers. (10.1109/ECTC.2009.5074124) (2009 May 26–29).
45. Chang, T. C., Hon, M. H. & Wang, M. C. Morphology and Phase Transformation at a Solder Jointin a Solid-State Reaction. *Electrochem. Solid-State Lett.* **7**, J4–J8 (2004).
46. Yoon, S. W., Choi, W. K. & Lee, H. M. Interfacial reaction between Sn–1Bi–5In-9Zn solder and Cu substrate. *Scripta Mater.* **40**, 327–32 (1999).
47. Liao, C. N. & Wei, C. T. An isochronal kinetic study of intermetallic compound growth in Sn/Cu thin film couples. *Thin Solid Films.* **515**, 2781–2785 (2006).
48. TANG, W. M., An-qiang, H. E., Liu, Q. & IVEY, D. G. Solid state interfacial reactions in electrodeposited Cu/Sn couples. *Trans. Nonferrous Met. Soc. China.* **20**, 90–96 (2010).
49. Rodriguez-Alvarez, H., Koetschaub, I. M., Genzela, C. & Schock, H. W. Growth paths for the sulfurization of Cu-rich Cu/In thin films. *Thin Solid Films.* **517**, 2140–2144 (2009).
50. Yan, C. *et al.* Kesterite Cu_2ZnSnS_4 solar cell from sputtered Zn/(Cu & Sn) metal stack precursors. *J. Alloys Compd.* **610**, 486–491 (2014).
51. Mitzi, D. B., Gunawan, O., Todorov, T. K., Wang, K. & Guha, S. The path towards a high-performance solution-processed kesterite solar cell. *Sol. Energy Mater. Sol. Cells* **95,** 1421–1436 (2011).
52. Katagiri, H. *et al.* Development of thin film solar cell based on Cu_2ZnSnS_4 thin films. *Sol. Energy Mater. Sol. Cells.* **65**, 141–148 (2001).
53. Shin, B. *et al.* Thin film solar cell with 8.4% power conversion efficiency using an earth-abundant Cu_2ZnSnS_4 absorber. *Prog. Photovolt: Res. Appl.* **21**, 72–66 (2011).
54. Wang, K. *et al.* Structural and elemental characterization of high efficiency Cu_2ZnSnS_4 solar cells. *Appl. Phys. Lett.* **98**, 051912 (2011).
55. Fernandes, P. A., Salomé, P. M. P. & da Cunha, A. F. Study of polycrystalline Cu_2ZnSnS_4 films by Raman scattering. *J. Alloys Compd.* **509**, 7600–7606 (2011).
56. Ge, J. *et al.* A 5.5% efficient co-electrodeposited ZnO/CdS/Cu_2ZnSnS_4/Mo thin film solar cell. *Sol. Energy Mater. Sol. Cells* **125**, 20–26 (2014).
57. Siebentritt, S. Why are kesterite solar cells not 20% efficient? *Thin Solid Films* **535**, 1–4 (2013).
58. Sousa, M. G. *et al.* Effect of rapid thermal processing conditions on the properties of Cu_2ZnSnS_4 thin films and solar cell performance. *Sol. Energy Mater. Sol. Cells* **126**, 101–106 (2014).
59. Fernandes, P. A. *et al.* Effects of sulphurization time on Cu_2ZnSnS_4 absorbers and thin films solar cells obtained from metallic precursors. *Sol. Energy Mater. Sol. Cells* **115**, 157–165 (2013).

Acknowledgments

This work is supported by "Aim for the Top university" under D103-33B04.

Author contributions

C.Y.S. contributed to the novelty and planning of this research, and solely conducted the experiments, characterizations, and analysis of the resulting data under the guidance J.M.T.. J.M.T. prepared figure 7 and C.Y.S. prepared the other figures. C.Y.C. provided advises of and participated in the electroplating. All authors reviewed this manuscript.

Additional information

Supplementary information accompanies this paper at http://www.nature.com/scientificreports

Competing financial interests: The authors declare no competing financial interests.

How to cite this article: Su, C.-Y., Chiu, C.-Y. & Ting, J.-M. Cu_2ZnSnS_4 absorption layers with controlled phase purity. *Sci. Rep.* 5, 9291; DOI:10.1038/srep09291 (2015).